nature sustainability

ARTICLES

https://doi.org/10.1038/s41893-021-00843-y

Check for updates

A large but transient carbon sink from urbanization and rural depopulation in China

Xiaoxin Zhang[1], Martin Brandt[1], Xiaowei Tong[1]✉, Philippe Ciais[2], Yuemin Yue[3,4]✉, Xiangming Xiao[5], Wenmin Zhang[1], Kelin Wang[3,4] and Rasmus Fensholt[1]

China has experienced unprecedented urbanization and associated rural depopulation during recent decades alongside a massive increase in the total population. By using satellite and demographical datasets, we here test the hypothesis that urbanization and carbon neutrality are not mutually exclusive and that sustainably managed urbanization may even be an integral part of the pathway to reduce atmospheric CO_2. We show that, although urban expansion caused an initial aboveground carbon loss of −0.02 PgC during 2002–2010, urban greening compensates these original losses with an overall balance of +0.03 PgC in urban areas during 2002–2019. We further show that a maximum increase in aboveground carbon stocks was observed at intermediate distances to rural settlements (2–4 km), reflecting the decreased pressure on natural resources. Consequently, rural areas experiencing depopulation (−14 million people yr^{-1}) coincided with an extensive aboveground carbon sink of 0.28 ± 0.05 PgC yr^{-1} during 2002–2019, while at the same time only a slight decline in cropland areas (4%) was observed. However, tree cover growth saturation limits the carbon removal capacity of forests and only a decrease in CO_2 emissions from fossil fuel burning will make the aim of carbon neutrality achievable.

The Earth is currently experiencing accelerating urbanization, with an unprecedented number of people moving from rural to urban areas[1]. This is particularly the case for emerging countries like China, which experienced the largest urbanization process in human history during recent decades[2]. At global scale, human population growth and urbanization have been shown to cause large losses in net primary production via the expansion of impervious surfaces and the conversion of natural and agricultural landscapes to built-up areas[3,4]. This process has been shown to cause considerable losses in ecosystem services[5], with shrinking biodiversity[6], losses of forests and carbon stocks[6,7], food security challenges[8] and increases in environmental pollution and CO_2 emissions[9].

Another aspect of urbanization is rural outmigration: while China's total population is one of the largest growing in the world (+8.46 million people yr^{-1} during 1980–2019), the share of China's rural population declined from 80.61% in 1980 to 39.40% in 2019, with over 290 million people moving to urban areas over the past three decades[10]. These numbers imply that ~6.90% of the global urban population in 2019 originates from rural areas and the real number is probably even higher, since many urban workers remain registered in their villages for the household registration system in China[11]. Rural depopulation has been linked with the term 'rural hollowing'[12], which entails abandonment of croplands/settlements and recovery of vegetation. Also, environmental degradation is an often-noted consequence of rural depopulation, meaning that food that was previously produced locally has to be imported, leading to increased pollution from international transportation and possible deforestation in other countries[13,14].

China has announced its plan to achieve carbon neutrality by 2060, which challenges current policies promoting the rapid urbanization of the entire country, as current per capita fossil CO_2 emissions rates are four times higher in urban than in rural areas[15]. However, several empirical studies have given evidence that rural outmigration can have a positive effect on vegetation production and carbon storage in rural regions[16,17]. Lowered human population densities reduce the pressure on natural resources, which potentially can lead to a recovery and densification of natural vegetation, especially if accompanied by environmental programmes that promote the restoration of degraded forests and landscapes with local species[18]. Several studies have identified China as a hot-spot of global greening and forest cover increase over the past decades[19,20], contradicting the perception that a rapid increase in population and urbanization could associate with degradation of vegetation.

With this background, we hypothesize that urbanization and the aim of carbon neutrality are not mutually exclusive and that sustainably managed urbanization may even be an integral part of the pathway to reduce net CO_2 emissions. However, for this hypothesis to be substantiated, favourable conditions need to be fulfilled, out of which the first three conditions are empirically tested here and the fourth condition remains a boundary condition for the study:

(1) Direct carbon losses caused by the conversion of vegetated areas to artificial surfaces need to be at least compensated by carbon gains from urban greening, for example by urban tree plantations. Urbanization areas (here defined as non-urban areas in 2000 but urban in 2020) should contribute to a net carbon removal.
(2) Rural outmigration areas should show a considerable gain in carbon sequestration. This can be both due to alleviated pressure on forests or the abandonment of croplands followed by woody vegetation encroachment. Ideally, rural outmigration should be accompanied by structured tree plantations and natural forest recovery programmes.

[1]Department of Geosciences and Natural Resource Management, University of Copenhagen, Copenhagen, Denmark. [2]Laboratoire des Sciences du Climat et de l'Environnement, CEA-CNRS-UVSQ, CE Orme des Merisiers, Gif sur Yvette, France. [3]Key Laboratory for Agro-ecological Processes in Subtropical Region, Institute of Subtropical Agriculture, Chinese Academy of Sciences, Changsha, China. [4]Huanjiang Observation and Research Station for Karst Ecosystem, Chinese Academy of Sciences, Huanjiang, China. [5]Department of Microbiology and Plant Biology, Center for Earth Observation and Modeling, University of Oklahoma, Norman, OK, USA. ✉e-mail: xit@ign.ku.dk; ymyue@isa.ac.cn

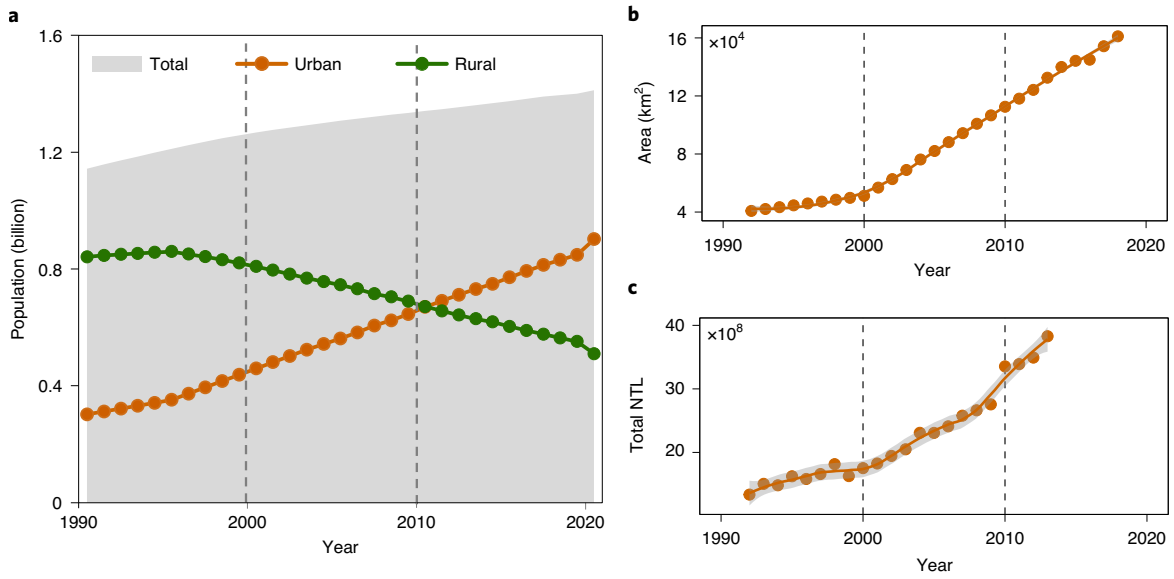

Fig. 1 | Population change and urbanization in China. a, Static demographic population. **b**, Urban areas based on ESA-CCI land cover (urban land cover class). **c**, Total NTL based on calibrated DMSP/OLS.

(3) The area of croplands should not decrease at the national scale to avoid massive food import causing deforestation and increased emissions in other countries.
(4) Fossil CO_2 emissions related to energy use caused by urban population growth and urbanization, should decrease. This is imperative, as an increase of the carbon sink will reach a point of saturation and would be offset by growing emissions, thereby making it impossible to achieve carbon neutrality.

To test the hypothesis that urbanization coincided with increased carbon sequestration from the four points listed, we used census, mobile phone location and population density data to estimate the spatiotemporal characteristics of rural–urban migration in China over recent decades (2000–2020). We further used satellite observations of night-time lights (NTL) and land cover maps to assess urbanization, as well as time series of satellite data on tree cover and aboveground biomass to analyse how rural–urban migration has been associated with carbon stock changes. If a relation between urbanization/rural outmigration and carbon stock increases exists, we expect new/relatively young forests around rural settlements with a shrinking population to recover faster than older forests in distance to those settlements that did not experience the same level of pressure in the past.

Results

Here, we study the relationship between urbanization, rural outmigration and changes in aboveground biomass. We structure the results according to the four points described above.

Greening of urban areas. China's total population increased from 1.13 billion to 1.40 billion (+24%) during 1990–2020, while rural population dramatically decreased (−28%) (Fig. 1a). Demographic data show an increase in China's rural population by +3.59 million people yr^{-1} from 1990 (841 million) to 1995 (859 million) followed by a strong decline resulting in only 510 million people remaining in rural areas in 2020 (a rural depopulation rate of −14 million people yr^{-1} during 2000–2020). At the same time, urban population increased from 301 million (26.41%) in 1990 to 848 million (63.89%) in 2020 (Fig. 1a). In 2011, the urban population exceeded the rural population for the first time. The annual European Space Agency and Climate Change Initiative (ESA-CCI) land cover classification[21] shows the massive expansion of the urban area class after 2000, which is supported by satellite data on NTL following the same pattern (Fig. 1b,c).

We aggregated 30 m of artificial surfaces from GlobeLand30 (ref. [22]) to 1-km^2 grids to subclassify urban areas into urban core (>50% artificial surfaces in 2000), mainly urban (>50% artificial surfaces in 2020 but ≤50% in 2000) and suburban (25–50% artificial surfaces in 2020). We further used annual aboveground biomass maps generated by Tong et al.[23] from optical moderate resolution imaging spectroradiometer (MODIS) and low-frequency passive microwave data to assess aboveground carbon stock dynamics in these areas. We find that all three urban classes saw a slight net increase in aboveground biomass over 2000–2019 (Fig. 2a,b). More precisely, carbon stocks in the three classes of urban areas decreased before 2010 but increased afterwards to reach a maximum in 2019 (0.40 PgC) as compared to the initial value biomass stock (0.36 PgC) in 2002 (Fig. 2c). Interestingly, the increase was strongest in the urban core areas (Fig. 2b). Overall, urban classes contributed a modest 2.60% to the total aboveground carbon stock increase in China over 2002–2019 (Fig. 2b,c).

Aboveground biomass in rural outmigration areas. To further study biomass changes in rural regions, we classified areas outside urban areas (see previous section for definitions) and towns with a low population density as 'agricultural land', which includes croplands and their surroundings (including rural settlements) (Fig. 2a,b,d). We further divided these areas into 'high agricultural pressure', which are 1 × 1 km^2 grid cells where croplands dominate (>50% cropland in 2000) and 'low agricultural pressure' (≤50% cropland in 2000), which are grids where forests and other land-covers dominate. The 'forest' class is dominated by forests (>50% in 2000) but can include smaller settlements and other land cover types as well. Agricultural land with low pressure has by far the strongest increase in biomass, followed by 'forests' and agricultural land with high pressure (Fig. 2b,d).

We then studied the changes in population migration and aboveground carbon density in relation to the distance to settlements, reflecting different intensity levels of human pressure (Fig. 3). Here, we used the static settlement map known as 'The Global

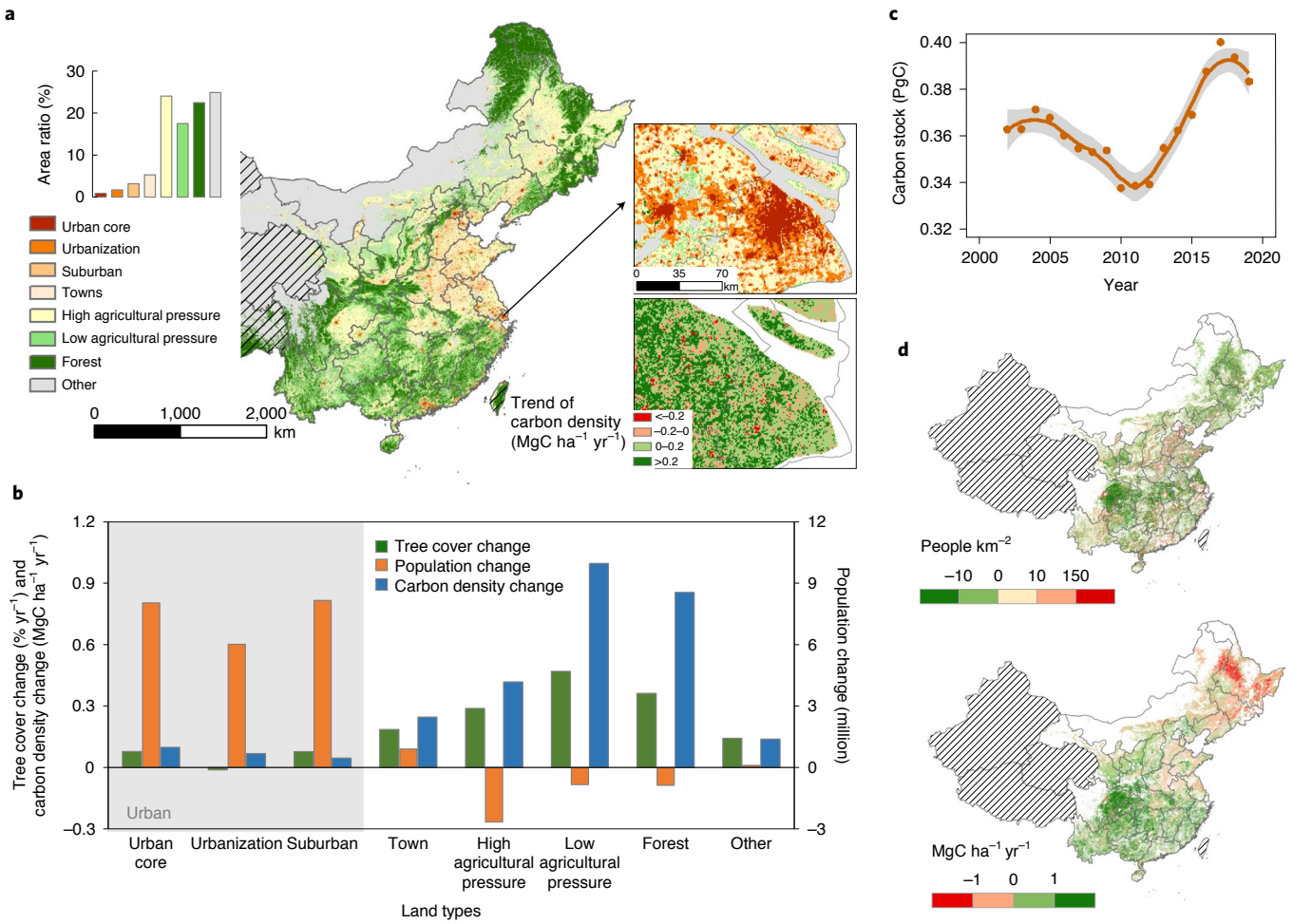

Fig. 2 | Land use/cover systems and MODIS carbon density change in China. a, Urban–agricultural–forest land systems (urban areas classified by artificial surfaces; Methods)**:** upper inset, example of land use/cover in Shanghai; lower inset, same as upper but for trends in carbon density. **b**, Mean tree cover change, mean carbon density change and population change for different land use/cover types for 2000–2020. **c**, Aboveground carbon stocks in urban areas (including urban core, urbanization and suburban, see **a**). **d**, Population density (upper map) and carbon density change (lower map) in agricultural land (including 'high agricultural pressure' and 'low agricultural pressure'; Methods). The western part of China with no/sparse vegetation and population (Xinjiang, Qinghai, Tibet) was excluded, shown as hatched areas.

Urban Footprint'[24], generated from radar satellite imagery at ~12-m spatial resolution. A maximum increase of aboveground biomass was observed in moderate distance (2–4 km) to settlements (Fig. 3a–d). This is because harvest activities before rural outmigration kept forests young and with a low carbon density, which now have a high capacity to recover and densify. At longer distances from settlements (>4 km), the smallest amount of regrowth was observed, as these more remote forest areas probably experienced less past disturbance, thereby showing a smaller potential for recovery.

Many people live in cities today but remain registered in their home villages, which causes a bias in the population density datasets used in this study. To circumvent this bias and to further support the migration patterns in relation to aboveground carbon density changes, we used daily mobile phone location data gridded at 1 km. Using these data from 2017 for a hot-spot area of biomass increase (Fig. 3e), we quantify the number of rural people living usually in cities, defined as the number of people who return to a rural home during the spring festival vacation period (Fig. 3f). The patterns of rural migration using this dataset, match the patterns of increasing aboveground carbon density (Fig. 3g).

To analyse aboveground biomass changes in relation to human migration, we used different groups of population density change (Table 1 and Fig. 4). Group 1 characterizes areas of large population density decline, group 2 shows minor decreases in population density, group 3 shows areas with minor increases in population density, group 4 covers areas with moderate population density increase and group 5 corresponds to areas of massive urbanization and population increase (Methods). Aboveground carbon density (Fig. 4a) shows clear differences of temporal trends among the five groups, with the highest increase in group 1 (0.71 MgC ha^{-1} yr^{-1}) and the lowest in group 5 (0.22 MgC ha^{-1} yr^{-1}) (Table 1 and Fig. 4a). Trends of different variables for the five groups were then compared for two time periods, before and after 2000, given that the year 2000 was identified as the year at which urbanization accelerated (Fig. 1). We included the advanced very-high-resolution radiometer (AVHRR)-based tree cover dataset[7] here to study the period before 2000, when no biomass data are available. During the early period (before 2000), trends in tree cover were similarly low for all groups (Fig. 4b) and also similar trends for NTL in all groups reflect the low level of urbanization during this period (Fig. 4c). After 2000, tree cover changes were highest in group 1 (Table 1) and NTL for areas with large population increases (group 5) reflect urbanization and population increase during the later period (Fig. 4b,c). The coarse resolution (5 km) of the AVHRR data (Fig. 4b) does not reveal the

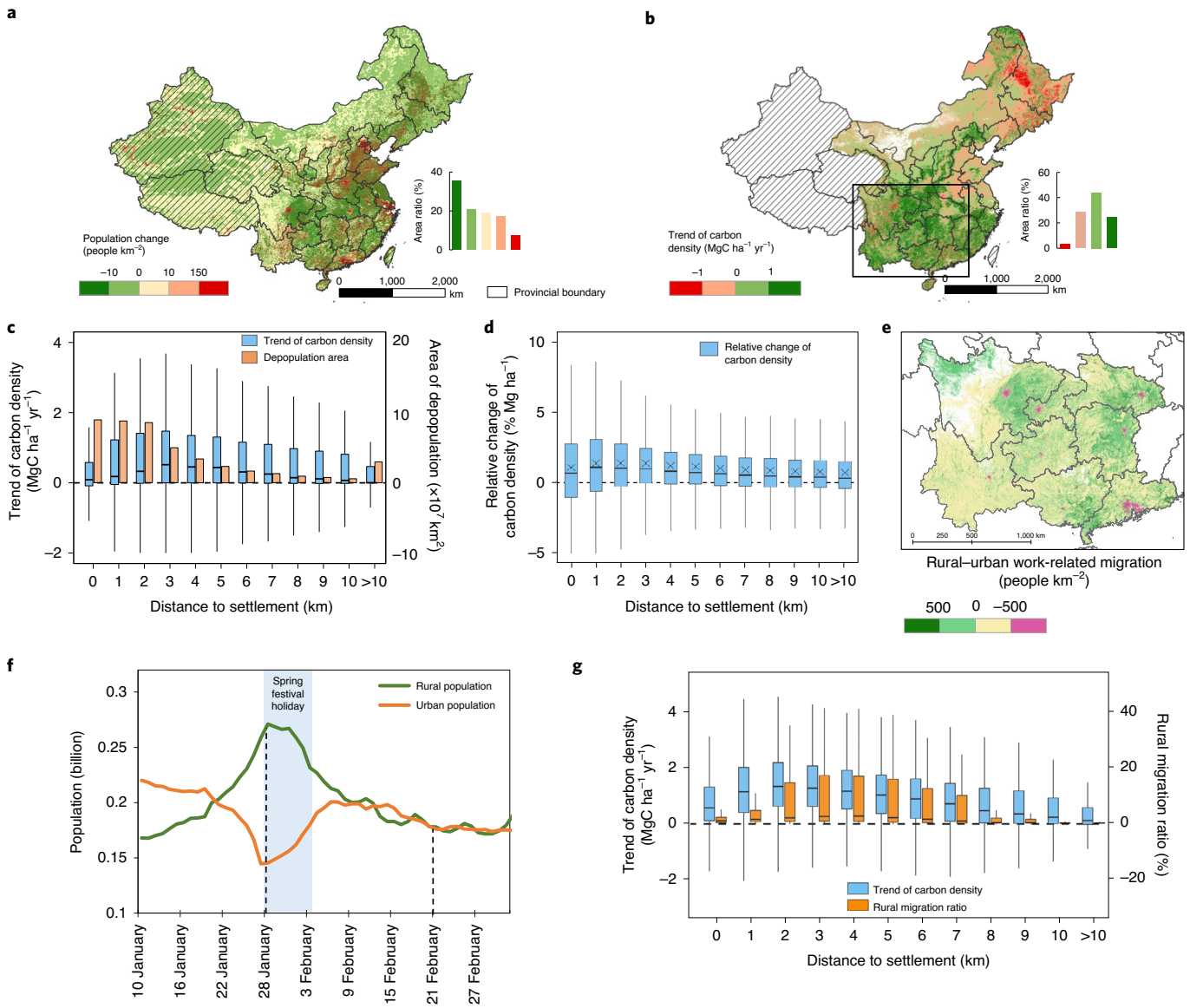

Fig. 3 | Population migration and aboveground carbon density change in relation to distance to settlements. a, Population density change for 2000–2020 based on WorldPop. **b**, Trend in MODIS-based aboveground carbon density for 2002–2019. The western part of China with no/sparse vegetation and population (Xinjiang, Qinghai, Tibet) was excluded, shown as hatched areas. **c**, Boxplot of aboveground carbon density change and area of depopulation for different distances to settlements. **d**, Relative change of aboveground carbon density (carbon density change/carbon density in 2002) for different distances to settlements (×, mean value; –, median value). The same pattern remains if only agricultural areas are considered (Extended Data Fig. 5). **e**, Population migration calculated from mobile phone location data, determined as the difference between the period of spring festival holidays (28 January) and after spring festival (21 February) for eight provinces. **f**, Rural and urban population change from mobile phone location data in 2017 for eight provinces during spring festival (urban and rural areas from Fig. 2a,b). **g**, Aboveground carbon density change and rural population migration ratio (population migration/population density after spring festival) from mobile phone location data for different distances to settlements for eight provinces shown in **e**. In the box plots the lower and upper box limits are the 25th and 75th percentiles, the central line is the median, and the upper (lower) whiskers extend to 1.5 (−1.5) times the interquartile range.

clear differences between the groups seen in the higher resolution MODIS data (Table 1 and Extended Data Fig. 1).

Taken together, these results support that rural outmigration areas can be associated with increases in aboveground carbon stocks.

Marginal decline of croplands. To quantify how urbanization reshaped the land systems, we used the GlobeLand30 land cover data and found that active croplands declined by 3.80% (68,164 km^2) from 2000 to 2020 in China (Extended Data Fig. 2). We further analysed which land cover types were replaced by artificial surfaces for the same period. Artificial surfaces replaced mainly croplands (81.00%), followed by grasslands (10.11%) and forests (6.01%) (Fig. 5a). The relatively low aboveground biomass of croplands helps explaining the overall increase of biomass in urbanization areas shown in the previous section. At the same time, new forests replaced grassland (59.48%), cropland (34.05%) and shrubland (4.35%) (Fig. 5a), mostly located in mountain areas[7] (Extended Data Fig. 3), explaining the biomass increase in rural areas. Even though urban areas mainly expanded into croplands, given the improved

Table 1 | Groups of population density changes and land cover change in China (2000–2020)

Group	Population density change (people km^{-2})	Area ratio (%)	Cropland (2000) (%)	Cropland change (2000–2020) (%)	Artificial surfaces (2000) (%)	Artificial surfaces change (2000–2020) (%)	Forest (2000) (%)	Tree cover change (% yr^{-1})	Carbon density change (MgC ha^{-1} yr^{-1})
1	<−10	35.58	53.39	−2.34	2.62	2.05	30.97	0.35	0.71
2	(−10, 0)	20.88	28.29	−1.48	0.56	0.56	45.77	0.35	0.69
3	(0, 10)	19.10	25.98	−1.17	0.67	0.74	41.26	0.31	0.67
4	(10, 150)	17.14	53.63	−3.96	4.30	3.78	26.20	0.28	0.57
5	≥150	7.30	61.66	−14.41	18.46	15.50	9.87	0.11	0.22

The population density difference between 2020 and 2000 was based on WorldPop population density maps. Land cover maps are derived from GlobeLand30. Tree cover change was derived from MOD44B. Aboveground carbon density change is derived from MODIS C density[23].

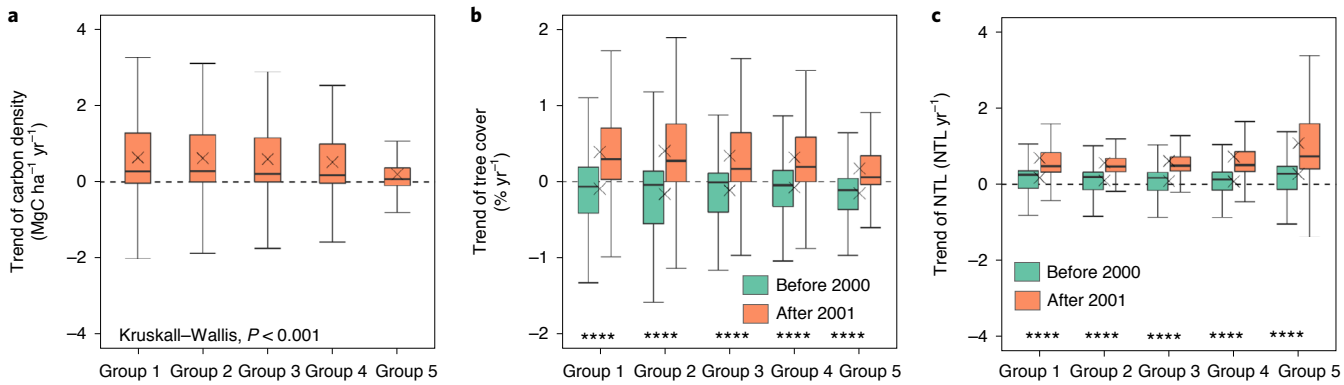

Fig. 4 | Comparison of tree cover, carbon density and NTL for grouped changes of population density in China for different periods. a, Trend of MODIS-based aboveground carbon density change (Methods). **b**, Trend of tree cover based on VCF5KYR. **c**, Trend of calibrated NTL. The groups reflect different changes in population density: group 1, <−10; group 2, (−10, 0); group 3, (0, 10); group 4, (10, 150); group 5, ≥150 (units are people km^{-2}). In **a**–**c**, ×, mean value; –, median value; significant differences between groups and periods were tested using the Kruskall–Wallis test, ****$P < 0.001$. The lower and upper box limits are the 25th and 75th percentiles, the central line is the median, and the upper (lower) whiskers extend to 1.5 (−1.5) times the interquartile range.

agricultural technologies and management[25,26], the decline in croplands is not expected to have major impacts on crop production and food security, also given the fact that most abandoned croplands were located on sloping hills with marginal soils[27].

Aboveground carbon sink and CO_2 emissions trends. Forest growth saturation limits the carbon removal capacity of forests in the long term. Indeed, while tree cover strongly increased over 2000–2011, the increase slowed down in recent years (Fig. 5b). Interestingly, while the net aboveground carbon sink continued to increase between 2012 and 2017 in our estimation, the rate of increase was close to zero in 2018 and 2019. At the same time, the increase of fossil CO_2 emissions also slowed down in 2011, with only a small growth rate in the last years. If the aboveground carbon gains are slowing down and are outpaced by the continuing growth of fossil CO_2 emissions, conditions for incepting a net-zero future pathway will not be met, unless further actions are taken to reduce emission strongly in the future.

Discussion

This study has tested the hypothesis that urbanization and rural depopulation in China promote aboveground carbon sinks that can contribute to carbon neutrality.

Urbanization is generally assumed to lead to an increased release of carbon to the atmosphere via the expansion of urban areas into forests and croplands, being primarily replaced by artificial surfaces with a limited carbon uptake[3,6]. Land cover types normally acting as a carbon sink are removed and the associated stored carbon is released. Yet, our results show that after an initial decrease, aboveground carbon stocks in urban expansion areas increased again (Fig. 2c), resulting in a neutral aboveground carbon balance over the full period of analysis. While this analysis excludes belowground carbon, the relatively low loss in aboveground carbon caused by urbanization is probably because cities have mostly expanded into croplands[4] (Fig. 5a and Extended Data Fig. 2); a land cover type representing a limited aboveground carbon stock. The increase in aboveground carbon observed in later years may be a sign of the phenomenon called urban greening, which includes tree plantings and the installation of green and community parks to supply the demand of green space and urban sustainability[28]. Since 2012, China started including 'ecological civilization'[29] into national plans and its constitution[30] and urban greening is an essential component of sustainable city planning[31,32]. All residential areas require a certain percentage of green space, most of them dominated by trees and shrubs, having a relatively high biomass[33]. While our results show that urban expansion can lead to a slight increase in aboveground biomass, the overall amount of sequestered carbon is small at national level and the future of this carbon sink is highly uncertain.

Rapid urbanization in China goes hand in hand with rural depopulation, which impacts on ecosystems and their services[6,13,34]. According to our results, more than half of all regions (59.71%) in China have witnessed a decline in population density during

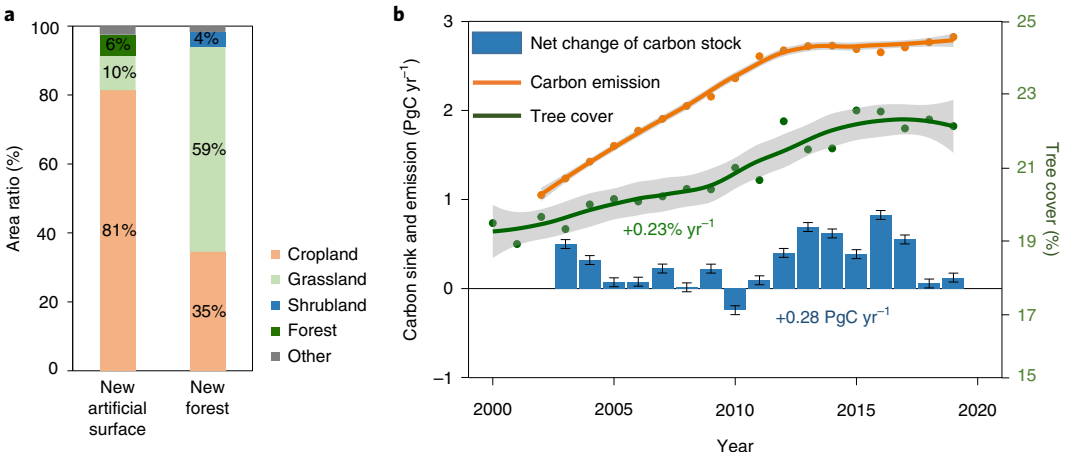

Fig. 5 | Land cover transitions and fossil carbon emissions in China. a, Loss of natural land from expanding areas of artificial surfaces and new forests replacing other land use/cover types based on GlobeLand30 land cover maps (2000, 2020). **b**, Annual net carbon change, annual carbon emissions from fossil fuel burning and annual tree cover are shown. The error bars represent the uncertainty of MODIS carbon density data.

2000–2020 (Fig. 3a). At the same time, we observed an increase in an aboveground carbon sequestration of $0.29 \pm 0.05\,PgC\,yr^{-1}$ at national level after 2002. This is not a new finding[19,35] and, even though total numbers vary, several studies have identified China as a global hot-spot of tree cover and biomass increase[20,36]. However, current understanding attributes this phenomenon solely to afforestation and reforestation activities[36,37]. Here, we find a relation between rural outmigration and biomass increase, with the strongest increases happening in areas with a declining population. This suggests that reduced human pressure on forests is an important factor contributing to recent biomass increases at the national level in China. Biomass increases in the vicinity of settlements were rather low, suggesting that tree plantation activities, which typically happen in close proximity to settlements, are not the dominant driver behind the large biomass increases. Also, biomass increases were low in areas further away from settlements, suggesting that external forcing (for example, CO_2 fertilization) is not dominant. Both afforestation/reforestation and rural depopulation are part of China's conservation policies, aiming at improving the environmental conditions in ecologically fragile areas, which is in particular the case for mountain regions[27,38]. The increased carbon stocks in rural areas are therefore not to be considered only a side effect of urbanization and a result of rural outmigration for increased welfare but part of national development strategy aiming at strengthening urban agglomeration areas and alleviating human pressures on rural and often degraded ecosystems. In addition, other factors contribute to aboveground biomass changes in China and population migration is certainly not always the dominant factor. For example, deforestation in northeast China counters possible biomass gains from rural depopulation[39]. Moreover, biomass increases accelerated after 2010. While this coincides with an accelerated urbanization rate (Fig. 1) and 2011 was also identified as the first year where urban population exceeds rural population, also climatic conditions improved after 2010 (Extended Data Fig. 4f), certainly contributing to the observed patterns.

Croplands have declined both from urban expansion, forestation and land abandonment. However, at national level, the overall decline was only 3.80% over the recent two decades, meaning that an extensive increase of international food imports is not expected as a consequence of changes in cropland areas (Extended Data Fig. 2). Still, the high demand of urban populations for imported products that possibly increase CO_2 emissions from land conversions elsewhere (for example, soybean plantations in South America[40]) and transport need to be considered[41].

An overall stagnation in the increase of tree cover and carbon stocks was observed in recent years, being in line with other studies on vegetation productivity in China[42]. Beside environmental factors (for example, CO_2 fertilization) that reached a natural limit[43], this may be related to the use of fast-growing species which dominated rural areas rapidly after the policies on tree plantation and urbanization were implemented in the year 2000. In later years, it is therefore likely that fast-growing tree cover has reached a point in time where their capacity for sequestering carbon has slowed down. This indicates that the large carbon sink caused by forest cover increases is unlikely to continue as in the past decades and, even though our results suggest that rapid urbanization and carbon neutrality are not mutually exclusive, a drastic reduction of CO_2 emissions from fossil fuel burning is pivotal in striving for carbon neutrality.

The aboveground carbon stock increases for China shown in this study covering 2002–2020 ($0.29\,PgC\,yr^{-1}$) are higher than those estimated by Piao et al.[44], who used inventory and ecological models to estimate a net carbon sink in China of 0.13–0.22 Pg C yr^{-1} for a former period in 1980–2002, of which 53% were contributed to by aboveground vegetation biomass. Pan et al.[45] found that China's forest area increased by 14% and the carbon density by 12% for 2000–2007, resulting in a carbon sink of $0.18\,PgC\,yr^{-1}$ based on forest inventory data. Our study showed a continuous increase of tree cover after 2007 (+2% at national level, Fig. 5), explaining the slightly higher number. Uncertainties in the temporal biomass carbon dynamics ($\pm 0.05\,PgC\,yr^{-1}$) were derived from an independent dataset based on low-frequency passive microwaves (L-VOD), with uncertainty being estimated by the root mean square error between L-VOD- and MODIS-derived carbon density estimates[23]. This gives confidence in the use of optical MODIS data, which includes large uncertainties of carbon dynamic for tropical forests with dense vegetation that shows low spectral variability in the spatial and temporal domain[46]. This is less problematic in China where vegetation is less dense[23], yet the interannual variation in our data is relatively high.

Our study uses multiple remote sensing data associated with demographical data and reveals that rural–urban migration based on policy implementations is an important factor leading to tree cover/biomass recovery in China. Rural–urban migration patterns in China can help to understand how urbanization combined with ecological restoration can alleviate human pressure from the environment and lead to increased carbon sequestration as a step towards reaching carbon neutrality[47], which is essential to achieving the UN's Sustainable Development Goals[48].

Methods

Multiple independent time-series datasets were applied to explore the impact of population migration on aboveground biomass changes in China. We used two independent datasets to evaluate tree cover dynamics. We further generated a dataset on aboveground biomass, following ref. [23]. Gridded population density maps, calibrated NTL, mobile phone location data and land cover maps are applied to reflect rural outmigration and urbanization.

Population density change. We used the gridded population density maps from WorldPop which are available for 2000 and 2020 to estimate human population density change. WorldPop uses random forest algorithms to weight and disaggregate the census data with geospatial covariates (for example, land cover) to produce gridded population at a resolution of 30 arcsec (~1 km at Equator), referred to as a 'top-down' modelling approach[49]. Mobile phone location data from 2017 were provided by the Tencent location service platform (the most popular internet service provider in China), gridded records at 1-km resolution and not including any personal information[50]. These data were generated by recording the position of individual mobile-phones' real-time when being used. We generated daily population density maps at $1\times1\,km^2$ for eight provinces of southern China, which were identified as hot-spot areas for this study. We calculated the difference in the population density maps between the first day during spring festival (28 January) and after the spring festival (28 February) to estimate rural–urban migration.

Dynamics of tree cover. Two vegetation continuous field (VCF) datasets were used to explore tree cover dynamics, namely, VCF5KYR derived from AVHRR LTDR[7] and MOD44B derived from C6 Terra MODIS[51]. VCF5KYR is available at 0.05° spatial resolution at yearly intervals from 1982 to 2016, providing fractional covers of trees, short vegetation and bare ground. Tree canopy cover refers to the proportion of ground covered by the vertical projection of tree crowns taller than 5 m in height[7]. The years 1994 and 2000 are missing and were here linearly interpolated on the basis of the previous and following years. The collection 6 of MOD44B is a yearly product presenting a continuous, subpixel fraction of land surface cover at a 250-m resolution from 2000 to 2019. Linear regression was used to estimate trends of tree cover at pixel level. The western part of China with no/sparse vegetation (Xinjiang, Qinghai, Tibet) and the less populated regions (population density <5 people km^{-2} in 2020) were excluded in statistical analyses.

Urbanization. NTL derived from the Defense Meteorological Program Operational Line-Scan System (DMSP/OLS) v.4 from 1992 to 2013 were used as a proxy of human activity. Due to the lack of calibration between the different satellites, we applied a calibration to create a continuous and comparable NTL time series. The details of the calibration process are found in ref. [52]. We also used the urban area class from the annual ESA-CCI 300-m land use dataset[21] to study urban expansion for 1992–2018.

Land cover. GlobaLand30 land cover maps with a spatial resolution of 30 m (2000, 2020) were used to define urban areas and agricultural land for 2000–2020. GlobaLand30 land cover maps are produced by the National Geomatics of China (NGCC) using Landsat satellite images[22]. The ten classes are: water, wetland, artificial surfaces, cultivated land, forest, shrubland, grassland, bare land, tundra and permanent snow/ice. The overall accuracy of the classification of 2020 is reported to be 85.72% (ref. [53]).

We use the classes 'artificial surfaces', 'cropland' and 'forest' to reflect a gradient from urban to rural, with different levels of human pressure. We work with $1\times1\,km^2$ grids and the percentage of the grid covered by a certain land cover class defines the urban/rural level: urban cores were defined as areas with artificial surfaces >50% in 2000. Urbanization areas were defined as areas with artificial surfaces >50% in 2020 but not in 2000. Suburban areas are grids with artificial surface covering 25–50% of the grid in 2020 and towns are areas where 15–25% are covered by artificial surfaces. We then classified areas outside of urban regions (urban core, urbanization and suburban) and towns having a low population density as 'agricultural land', which includes croplands and their surroundings (including rural settlements). We further divided these areas into 'high agricultural pressure', which are $1\times1\,km^2$ grids where croplands dominate (>50% cropland in 2000) and 'low agricultural pressure' (≤50% cropland in 2000), which are grids where forests and other land-covers dominate. The 'forest' class is dominated by forests (>50% in 2000). Rural area is defined as the whole region that is located outside of urban regions in the study, including towns, agricultural land, forest and other land.

Carbon density. We used the dataset from ref. [23] on annual aboveground carbon density, expanded to all China. The dataset used a static benchmark map of aboveground biomass from ref. [54] reflecting the situation around 2018 to train a random forest algorithm applied on annual MODIS MCD43A4 BRDF corrected imagery (collection 6) at 1-km resolution. The annual maps were created from daily images using the median and then a moving median window over 3 yr, to guarantee cloud and noise-free annual images. We used all seven bands of the MCD43A4 product, plus the EVI2, the NDII and the MCD43A3 shortwave albedo and a SRTM elevation model to train the model, following ref. [55]. We used 10% ($n=791{,}726$) of the pixels of an averaged (2002–2019) image to train the model and the remaining 90% for validation. We refer to ref. [54] for information on the static biomass map and to ref. [23] for more information on the dynamic product. Independent evaluation was conducted with SMOS-based passive microwave L-VOD time series (2010–2019), which is currently the only satellite-based dataset able to reliably quantify aboveground biomass dynamics. Due to low data quality of the SMOS satellite in northern China, the evaluation could only be performed for eight provinces of southern China, which is, however, assumed to be sufficient, as a majority of the forest ecosystems in China are located in these regions. The comparison of the aboveground biomass dynamics between the L-VOD-based and the MODIS-based product showed a high agreement ($r=0.7$ at spatial and $r=0.9$ at temporal level). The root mean square error was 0.05 PgC yr^{-1}, which we use here to report the uncertainty. More details on the evaluation process are found in ref. [23]. The random forest model was applied to each year to estimate changes in biomass carbon density for 2002–2019.

Other datasets. Demographic data from the national census shows rural and urban residents at annual scale for the whole country from 1990 to 2020. Global Urban footprint (GUF) dataset provides human settlement map with ~12-m spatial resolution. Fossil CO_2 emission data derived from Global Carbon Project[56], were used to evaluate fossil CO_2 emission at national scale for 2000–2019. We converted CO_2 emission to carbon emission by dividing the values by 3.67.

Reporting Summary. Further information on research design is available in the Nature Research Reporting Summary linked to this article.

Data availability

Population density data from WorldPop (2000–2020) can be obtained at https://www.worldpop.org. Demographical data are accessible from the National Bureau of Statistics of the People's Republic of China. Tree cover from AVHRR (VCF5KYR) can be downloaded from https://search.earthdata.nasa.gov. Tree cover from MODIS (MOD44B) is available from Google Earth Engine. DMSP/OLS Nighttime Lights Time Series Version 4 can be download from https://ngdc.noaa.gov/eog/dmsp/downloadV4composites.html. GlobaLand30 land cover dataset is available at http://www.globallandcover.com/home_en.html. ESA-CCI land cover dataset is available at http://maps.elie.ucl.ac.be/CCI/viewer/. The MODIS carbon density map and mobile phone location-based dataset are available on request.

Code availability

No custom codes were used. The codes used to analyse the data and create the plot are available on request.

Received: 7 December 2020; Accepted: 13 December 2021;
Published online: 07 February 2022

References

1. Montgomery, M. R. The urban transformation of the developing world. *Science* **319**, 761–764 (2008).
2. Zhang, K. H. & Shunfeng, S. Rural–urban migration and urbanization in China: evidence from time-series and cross-section analyses. *China Econ. Rev.* **14**, 386–400 (2003).
3. Liu, X. et al. Global urban expansion offsets climate-driven increases in terrestrial net primary productivity. *Nat. Commun.* **10**, 5558 (2019).
4. Liu, X. et al. High-spatiotemporal-resolution mapping of global urban change from 1985 to 2015. *Nat. Sustain.* **3**, 564–570 (2020).
5. Cumming, G. S. et al. Implications of agricultural transitions and urbanization for ecosystem services. *Nature* **515**, 50–57 (2014).
6. Seto, K. C., Güneralp, B. & Hutyra, L. R. Global forecasts of urban expansion to 2030 and direct impacts on biodiversity and carbon pools. *Proc. Natl Acad. Sci. USA* **109**, 16083–16088 (2012).
7. Song, X. P. et al. Global land change from 1982 to 2016. *Nature* **560**, 639–643 (2018).
8. Barthel, S. et al. Global urbanization and food production in direct competition for land: leverage places to mitigate impacts on SDG2 and on the Earth system. *Anthr. Rev.* **6**, 71–97 (2019).
9. Zhou, L. et al. Evidence for a significant urbanization effect on climate in China. *Proc. Natl Acad. Sci. USA* **101**, 9540–9544 (2004).
10. Council, D. R. C. O. T. S. & Bank, T. W. *Urban China: Toward Efficient, Inclusive, and Sustainable Urbanization* (World Bank Group, 2014).
11. Chan, K. W. & Zhang, L. The hukou system and rural-urban migration in China: processes and changes. *China Q.* **160**, 818–855 (1999).
12. Liu, Y., Liu, Y., Chen, Y. & Long, H. The process and driving forces of rural hollowing in China under rapid urbanization. *J. Geog. Sci.* **20**, 876–888 (2010).
13. van Vliet, J. Direct and indirect loss of natural area from urban expansion. *Nat. Sustain* **2**, 755–763 (2019).
14. DeFries, R. S., Rudel, T., Uriarte, M. & Hansen, M. Deforestation driven by urban population growth and agricultural trade in the twenty-first century. *Nat. Geosci.* **3**, 178–181 (2010).

15. Wang, R. et al. High-resolution mapping of combustion processes and implications for CO_2 emissions. *Atmos. Chem. Phys.* **13**, 5189–5203 (2013).
16. Li, W. & Tan, M. Influences of vertical differences in population emigration on mountainous vegetation greenness: a case study in the Taihang Mountains. *Sci. Rep.* **8**, 16954 (2018).
17. Li, W., Li, X., Tan, M. & Wang, Y. Influences of population pressure change on vegetation greenness in China's mountainous areas. *Ecol. Evol.* **7**, 9041–9053 (2017).
18. Liu, J., Li, S., Ouyang, Z., Tam, C. & Chen, X. Ecological and socioeconomic effects of China's policies for ecosystem services. *Proc. Natl Acad. Sci. USA* **105**, 9477–9482 (2008).
19. Chen, C. et al. China and India lead in greening of the world through land-use management. *Nat. Sustain.* **2**, 122–129 (2019).
20. Wang, J. et al. Large Chinese land carbon sink estimated from atmospheric carbon dioxide data. *Nature* **586**, 720–723 (2020).
21. Defourny, P. et al. *Land Cover CCI: Product User Guide v.2* (UCL-Geomatics, 2012).
22. Chen, J. et al. Global land cover mapping at 30 m resolution: a POK-based operational approach. *ISPRS J. Photogramm. Remote Sens.* **103**, 7–27 (2015).
23. Tong, X. et al. Forest management in southern China generates short term extensive carbon sequestration. *Nat. Commun.* **11**, 129 (2020).
24. Esch, T. et al. Breaking new ground in mapping human settlements from space—The Global Urban Footprint. *ISPRS J. Photogramm. Remote Sens.* **134**, 30–42 (2017).
25. Zuo, L. et al. Progress towards sustainable intensification in China challenged by land-use change. *Nat. Sustain.* **1**, 304–313 (2018).
26. Wang, S. et al. Urbanization can benefit agricultural production with large-scale farming in China. *Nat. Food* **2**, 183–191 (2021).
27. Yue, Y. et al. Large scale reforestation of farmlands on sloping hills in South China karst. *Landsc. Ecol.* **35**, 1445–1458 (2020).
28. Zhang, W. et al. Socio-economic and climatic changes lead to contrasting global urban vegetation trends. *Glob. Environ. Change* **71**, 102385 (2021).
29. Gare, A. China and the struggle for ecological civilization. *Capitalism Nat. Social.* **23**, 10–26 (2012).
30. Feng, D., Bao, W., Yang, Y. & Fu, M. How do government policies promote greening? Evidence from China. *Land Use Policy* **104**, 105389 (2021).
31. Yao, N. et al. Beijing's 50 million new urban trees: strategic governance for large-scale urban afforestation. *Urban For. Urban Green.* **44**, 126392 (2019).
32. Li, F., Wang, R., Liu, X. & Zhang, X. Urban forest in China: development patterns, influencing factors and research prospects. *Int. J. Sustain. Dev. World Ecol.* **12**, 197–204 (2005).
33. Strohbach, M. W., Arnold, E. & Haase, D. The carbon footprint of urban green space—a life cycle approach. *Landsc. Urban Plan.* **104**, 220–229 (2012).
34. Seto, K. C. et al. Urban land teleconnections and sustainability. *Proc. Natl Acad. Sci. USA* **109**, 7687–7692 (2012).
35. Piao, S. et al. Characteristics, drivers and feedbacks of global greening. *Nat. Rev. Earth Environ.* https://doi.org/10.1038/s43017-019-0001-x (2019).
36. Ahrends, A. et al. China's fight to halt tree cover loss. *Proc. R. Soc. B* https://doi.org/10.1098/rspb.2016.2559 (2017).
37. Tong, X. W. et al. Increased vegetation growth and carbon stock in China karst via ecological engineering. *Nat. Sustain.* **1**, 44–50 (2018).
38. Zhang, Q. et al. Divergent socioeconomic-ecological outcomes of Chinaas conversion of cropland to forest program in the subtropical mountainous area and the semi-arid loess plateau. *Ecosyst. Serv.* **45**, 101167 (2020).
39. Yu, D. et al. Forest management in northeast China: history, problems, and challenges. *Environ. Manag.* **48**, 1122–1135 (2011).
40. Song, X.-P. et al. Massive soybean expansion in South America since 2000 and implications for conservation. *Nat. Sustain.* **4**, 784–792 (2021).
41. Meyfroidt, P., Rudel, T. K. & Lambin, E. F. Forest transitions, trade, and the global displacement of land use. *Proc. Natl Acad. Sci. USA* **107**, 20917–20922 (2010).
42. Ma, J. et al. Trends and controls of terrestrial gross primary productivity of China during 2000–2016. *Environ. Res. Lett.* **14**, 084032 (2019).
43. Wang, S. et al. Recent global decline of CO_2 fertilization effects on vegetation photosynthesis. *Science* **370**, 1295–1300 (2020).
44. Piao, S. et al. The carbon balance of terrestrial ecosystems in China. *Nature* **458**, 1009–1013 (2009).
45. Pan, Y. et al. A large and persistent carbon sink in the world's forests. *Science* **333**, 988–993 (2011).
46. Hansen, M. C., Potapov, P. & Tyukavina, A. Comment on "Tropical forests are a net carbon source based on aboveground measurements of gain and loss". *Science* **363**, eaar629 (2019).
47. Mallapaty, S. How China could be carbon neutral by mid-century. *Nature* **586**, 482–483 (2020).
48. Griggs, D. et al. Sustainable development goals for people and planet. *Nature* **495**, 305–307 (2013).
49. Tatem, A. J. WorldPop, open data for spatial demography. *Sci. Data* **4**, 170004 (2017).
50. Xu, Y., Song, Y., Cai, J. & Zhu, H. Population mapping in China with Tencent social user and remote sensing data. *Appl. Geogr.* **130**, 102450 (2021).
51. DiMiceli, C. M. et al. *Annual Global Automated MODIS Vegetation Continuous Fields (MOD44B) at 250 m Spatial Resolution for Data Years Beginning Day 65, 2000–2014, Collection 5 Percent Tree Cover, Version 6* (Univ. Maryland, 2017).
52. Zhang, X. et al. Urbanization and spillover effect for three megaregions in China: evidence from DMSP/OLS nighttime lights. *Remote Sens.* **10**, 1888 (2018).
53. Chen, F. et al. A landscape shape index-based sampling approach for land cover accuracy assessment. *Sci. China Earth Sci.* **59**, 2263–2274 (2016).
54. Saatchi, S. S. et al. Benchmark map of forest carbon stocks in tropical regions across three continents. *Proc. Natl Acad. Sci. USA* **108**, 9899–9904 (2011).
55. Cook-Patton, S. C. et al. Mapping carbon accumulation potential from global natural forest regrowth. *Nature* **585**, 545–550 (2020).
56. Friedlingstein, P. et al. Global carbon budget 2020. *Earth Syst. Sci. Data* **12**, 3269–3340 (2020).

Acknowledgements

X.Z. is funded by the National Natural Science Foundation of China (41930652) and China Scholarship Council (CSC, grant no. 201904910835). M.B. received funding from the DFF Sapere Aude (9064-00049B) and the European Research Council under the European Union's Horizon 2020 Research and Innovation Programme (TOFDRY, grant agreement no. 947757). X.T. is funded by a Marie Curie fellowship (795970). Y.Y. is funded by the National Natural Science Foundation of China (41930652, U20A2048). X.X. is supported by the US National Science Foundation (1911955). R.F. is supported by the Villum Foundation through the project 'Deep Learning and Remote Sensing for Unlocking Global Ecosystem Resource Dynamics' (DeReEco) (project no. 34306).

Author contributions

X.Z., M.B. and Y.Y. designed the research. X.Z. conducted experiments and analysis. MODIS C density was prepared by M.B. and X.T. Mobile phone location dataset was prepared and provided by Y.Y. and K.W. The paper was drafted by X.Z., M.B., P.C., X.T. and R.F. All co-authors discussed the results and contributed to the interpretation and revision of the final manuscript.

Competing interests

The authors declare no competing interests.

Additional information

Extended data is available for this paper at https://doi.org/10.1038/s41893-021-00843-y.

Supplementary information The online version contains supplementary material available at https://doi.org/10.1038/s41893-021-00843-y.

Correspondence and requests for materials should be addressed to Xiaowei Tong or Yuemin Yue.

Peer review information *Nature Sustainability* thanks Richard Houghton, Zhu Liu and the other, anonymous, reviewer(s) for their contribution to the peer review of this work.

Reprints and permissions information is available at www.nature.com/reprints.

Publisher's note Springer Nature remains neutral with regard to jurisdictional claims in published maps and institutional affiliations.

© The Author(s), under exclusive licence to Springer Nature Limited 2022

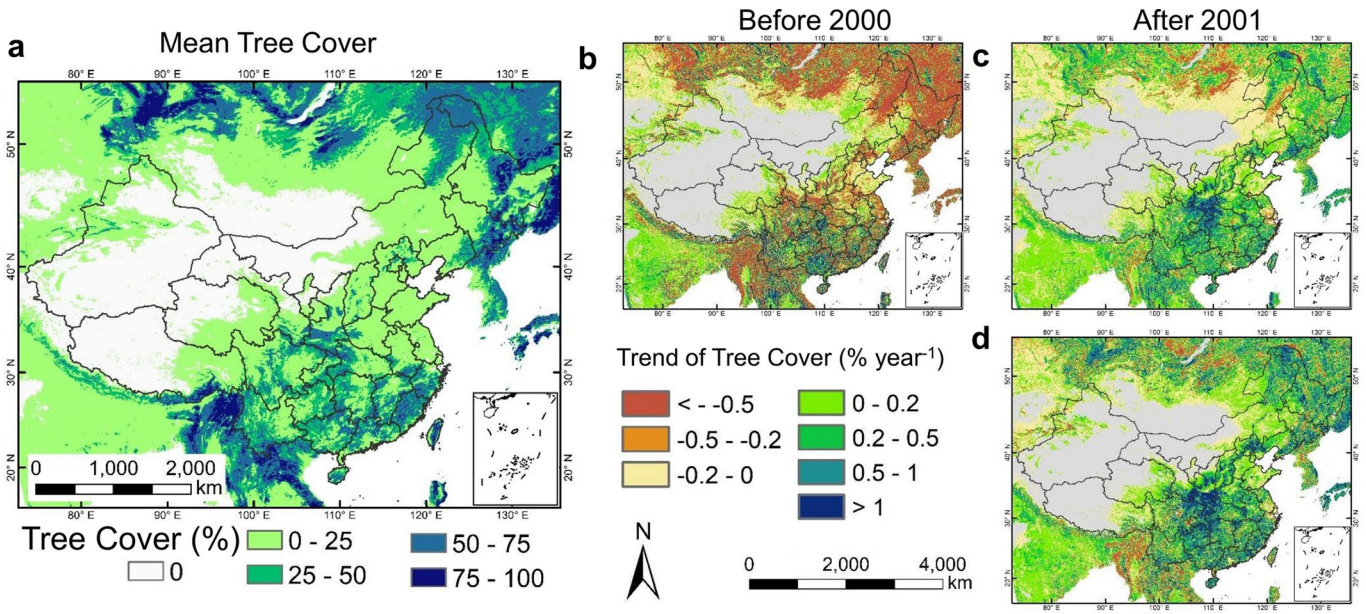

Extended Data Fig. 1 | Dynamic of tree cover in China. Dynamic of tree cover in China. **a**, AVHRR VCF5KYR tree cover for 2001[1]; **b**, trends of AVHRR VCF5KYR tree cover before 2000[1]; **c**, trends of AVHRR VCF5KYR tree cover after 2001[1]; **d**, Trends of MOD44B tree cover after 2001.

		2020 (Area: km^2)									
		Cropland	Forest	Grassland	Shrubland	Wetland	Water	Artificial surfaces	Bare land	Permanent snow and ice	Sum
2000 (Area: km^2)	Cropland	1603547	64173	57577	1814	2676	18496	110690	1072	0	1860046
	Forest	66221	1655273	95687	8378	421	5830	8176	757	147	1840891
	Grassland	78051	110637	974356	12937	3641	5197	13753	26018	1158	1225748
	Shrubland	2721	8083	7905	19591	117	237	345	443	1	39444
	Wetland	4023	342	4059	78	18714	5646	485	895	0	34243
	Water	13849	2183	2732	140	2813	63344	3404	653	1	89120
	Artificial surfaces	20342	941	1683	55	79	666	110028	114	0	133907
	Bare land	3127	279	44937	340	289	893	1282	463195	717	515059
	Permanent snow and ice	0	311	944	36	0	3	0	200	2068	3562
	Sum	1791882	1842222	1189881	43368	28749	100312	248163	493348	4093	
	Change (2000-2020)	**-68164**	**1332**	**-35867**	**3925**	**-5494**	**11193**	**114255**	**-21711**	**532**	
	Percent of change	**-3.80%**	**0.07%**	**-3.01%**	**9.05%**	**-19.11%**	**11.16%**	**46.04%**	**-4.40%**	**12.99%**	

Extended Data Fig. 2 | Land cover transition in China from GlobeLand30 during 2000–2020. Land cover transition in China from GlobeLand30 during 2000–2020.

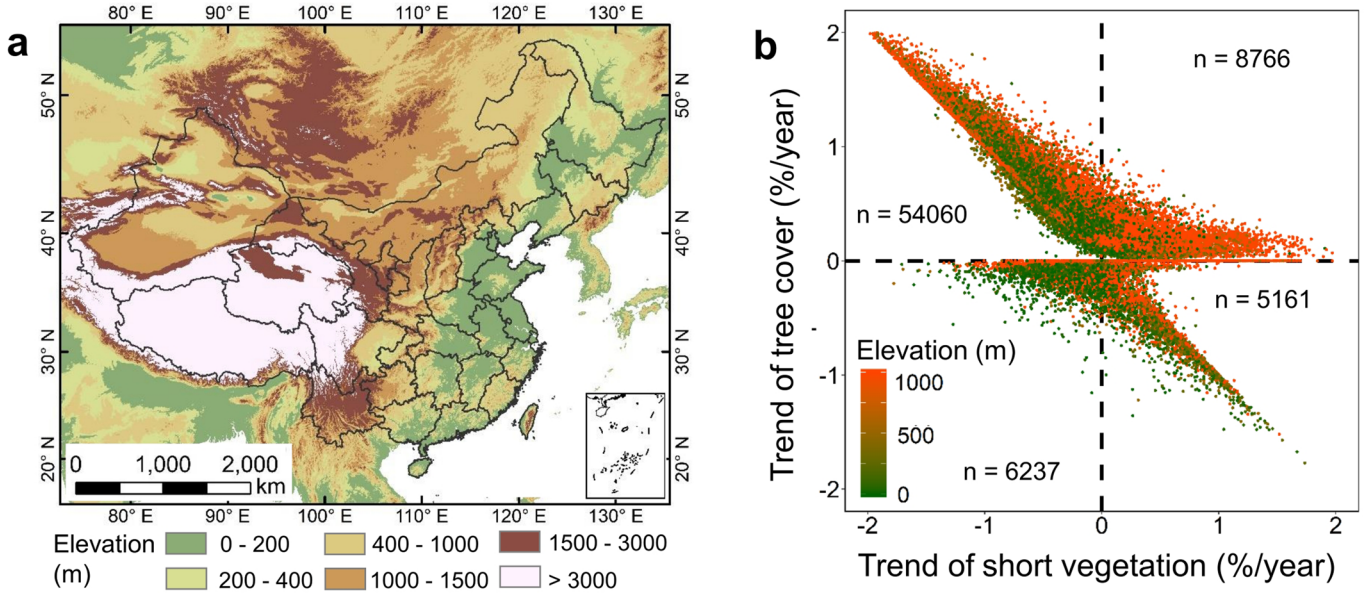

Extended Data Fig. 3 | Topography and vegetation trends. Topography and vegetation trends. **a**, Topography; **b**, significant change ($P < 0.05$) in tree cover, trends of short vegetation from AVHRR VCF5KYR[1], and elevation for 1990-2016.

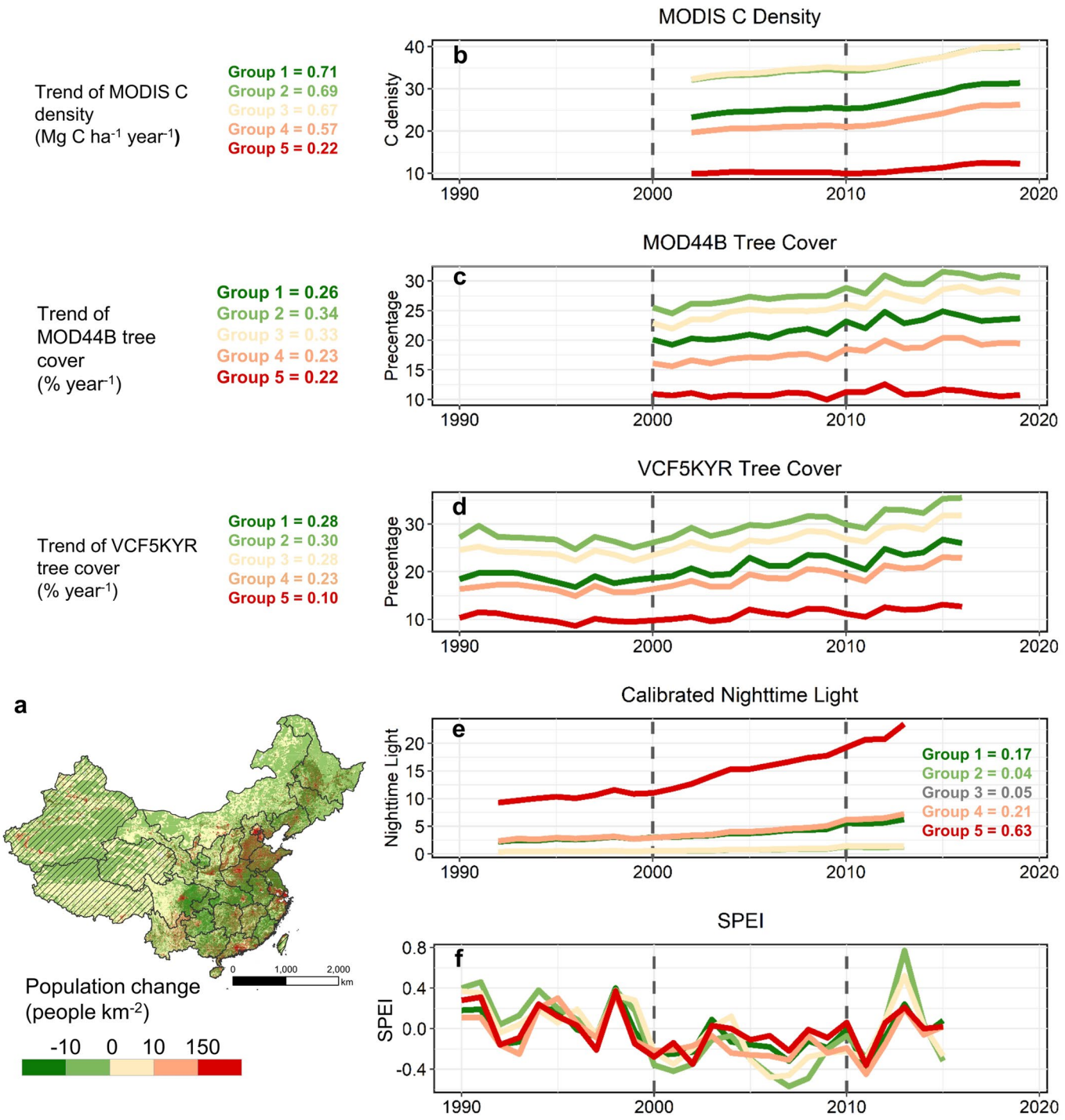

Extended Data Fig. 4 | Trends and temporal profiles separated in groups of population density change for 2000–2020. Trends and temporal profiles separated in groups of population density change for 2000–2020. **a**, Spatial distribution of each group of population density change based on WorldPop population density (2000,2020); **b**, MODIS-based aboveground carbon density; **c**, MOD44B tree cover; **d**, AVHRR VCF5KYR tree cover; **e**, calibrated nighttime light from DMSP/OLS; **f**, yearly mean Standardized Precipitation-Evapotranspiration Index (SPEI).

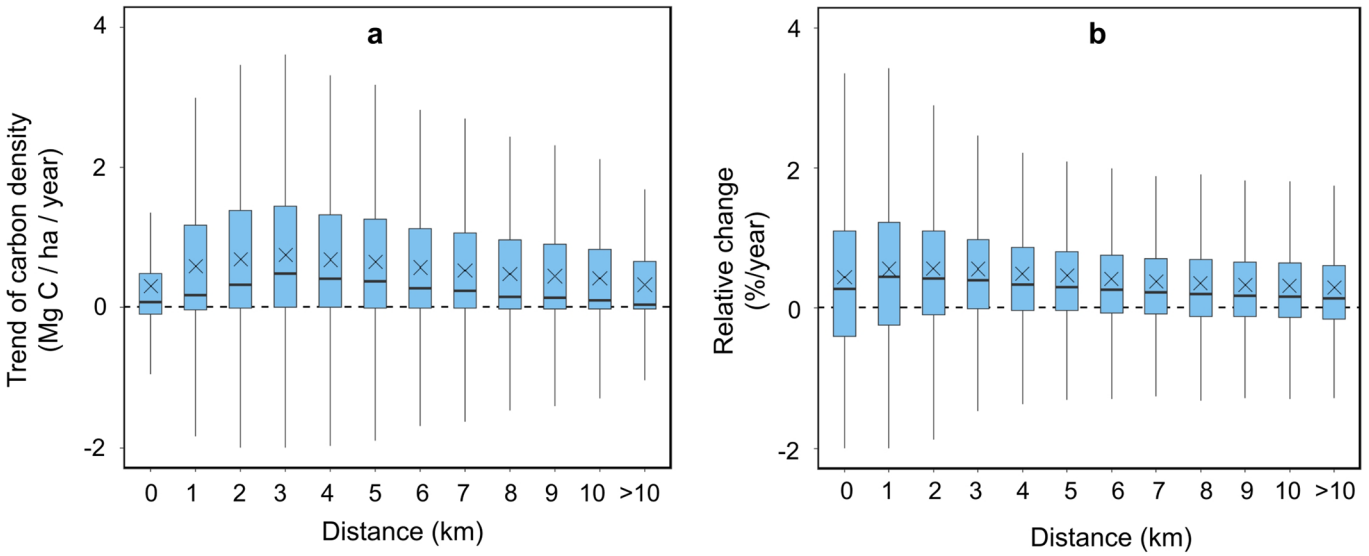

Extended Data Fig. 5 | Boxplots showing changes in carbon density in relation to distance to settlements in agricultural areas over China (× mean value, - median value). Boxplots showing changes in carbon density in relation to distance to settlements in agricultural areas over China (× mean value, - median value). **a**, MODIS-Based aboveground carbon density change for different distance to settlement; **b**, relative aboveground carbon density change (carbon density change / carbon density in 2002) in relation to distance to settlements.

nature portfolio

Corresponding author(s): DBPR, NATSUSTAIN-20128315B

Last updated by author(s): Nov 23, 2021

Reporting Summary

Nature Portfolio wishes to improve the reproducibility of the work that we publish. This form provides structure for consistency and transparency in reporting. For further information on Nature Portfolio policies, see our Editorial Policies and the Editorial Policy Checklist.

Statistics

For all statistical analyses, confirm that the following items are present in the figure legend, table legend, main text, or Methods section.

n/a	Confirmed	
☒	☐	The exact sample size (*n*) for each experimental group/condition, given as a discrete number and unit of measurement
☒	☐	A statement on whether measurements were taken from distinct samples or whether the same sample was measured repeatedly
☒	☐	The statistical test(s) used AND whether they are one- or two-sided *Only common tests should be described solely by name; describe more complex techniques in the Methods section.*
☒	☐	A description of all covariates tested
☐	☒	A description of any assumptions or corrections, such as tests of normality and adjustment for multiple comparisons
☐	☒	A full description of the statistical parameters including central tendency (e.g. means) or other basic estimates (e.g. regression coefficient) AND variation (e.g. standard deviation) or associated estimates of uncertainty (e.g. confidence intervals)
☒	☐	For null hypothesis testing, the test statistic (e.g. *F*, *t*, *r*) with confidence intervals, effect sizes, degrees of freedom and *P* value noted *Give P values as exact values whenever suitable.*
☒	☐	For Bayesian analysis, information on the choice of priors and Markov chain Monte Carlo settings
☒	☐	For hierarchical and complex designs, identification of the appropriate level for tests and full reporting of outcomes
☒	☐	Estimates of effect sizes (e.g. Cohen's *d*, Pearson's *r*), indicating how they were calculated

Our web collection on statistics for biologists contains articles on many of the points above.

Software and code

Policy information about availability of computer code

Data collection	Most datasets are downloaded from sources using web browsers, and MODSI-based aboveground biomass and mobile phone location dataset are provided by co-authors.
Data analysis	Data processing is carried out in RStudio (1.2) , ArcGIS Destop(10.6.1).

For manuscripts utilizing custom algorithms or software that are central to the research but not yet described in published literature, software must be made available to editors and reviewers. We strongly encourage code deposition in a community repository (e.g. GitHub). See the Nature Portfolio guidelines for submitting code & software for further information.

Data

Policy information about availability of data

All manuscripts must include a data availability statement. This statement should provide the following information, where applicable:

- Accession codes, unique identifiers, or web links for publicly available datasets
- A description of any restrictions on data availability
- For clinical datasets or third party data, please ensure that the statement adheres to our policy

Population density from WorldPop (2000-2020) can be obtained at https://www.worldpop.org. Demographics is accessible from the National Bureau of Statistics of the People's Republic of China. Tree cover from AVHRR (VCF5KYR) can be downloaded from https://search.earthdata.nasa.gov. Tree cover from MODIS (MOD44B) was available from Google Earth Engine. DMSP/OLS Nighttime Lights Time Series Version 4 can be download from https://ngdc.noaa.gov/eog/dmsp/downloadV4composites.html. GlobaLand30 land cover dataset is available at http://www.globallandcover.com/home_en.html. ESA-CCI land cover dataset is available at http://maps.elie.ucl.ac.be/CCI/viewer/. The MODIS carbon density map and mobile location-based dataset are available upon request.

Field-specific reporting

Please select the one below that is the best fit for your research. If you are not sure, read the appropriate sections before making your selection.

☐ Life sciences ☐ Behavioural & social sciences ☒ Ecological, evolutionary & environmental sciences

For a reference copy of the document with all sections, see nature.com/documents/nr-reporting-summary-flat.pdf

Ecological, evolutionary & environmental sciences study design

All studies must disclose on these points even when the disclosure is negative.

Study description	This study has tested the hypothesis that urbanization and rural depopulation in China promote aboveground carbon sinks that can contribute to carbon neutrality using multiply datasets.
Research sample	The study explored the effect of rural-urban migration on aboveground biomass in China using statistic-based and satellited-based gridded datasets.
Sampling strategy	NA
Data collection	Most datasets are downloaded by web browers from data sources. Population density from WorldPop (2000-2020) can be obtained at https://www.worldpop.org. Demographics is accessible from the National Bureau of Statistics of the People's Republic of China. Tree cover from AVHRR (VCF5KYR) can be downloaded from https://search.earthdata.nasa.gov. Tree cover from MODIS (MOD44B) was available from Google Earth Engine. DMSP/OLS Nighttime Lights Time Series Version 4 can be download from https://ngdc.noaa.gov/eog/dmsp/downloadV4composites.html. GlobaLand30 land cover dataset is available at http://www.globallandcover.com/home_en.html. ESA-CCI land cover dataset is available at http://maps.elie.ucl.ac.be/CCI/viewer/. The MODIS carbon density map and mobile location-based dataset are available from the corresponding authors.
Timing and spatial scale	We use the WorldPop-based population change and MODIS-based aboveground during 2000-2020 with the spatial resolution of 1*1km for China.
Data exclusions	The western part of China with no/sparse vegetation (Xinjiang, Qinghai, Tibet) and the less populated regions (population density < 5 people per km in 2020) were excluded in statistical analyses.
Reproducibility	All results are being processed many time.
Randomization	NA
Blinding	NA

Did the study involve field work? ☐ Yes ☒ No

Reporting for specific materials, systems and methods

We require information from authors about some types of materials, experimental systems and methods used in many studies. Here, indicate whether each material, system or method listed is relevant to your study. If you are not sure if a list item applies to your research, read the appropriate section before selecting a response.

Materials & experimental systems

n/a	Involved in the study
☒	☐ Antibodies
☒	☐ Eukaryotic cell lines
☒	☐ Palaeontology and archaeology
☒	☐ Animals and other organisms
☒	☐ Human research participants
☒	☐ Clinical data
☒	☐ Dual use research of concern

Methods

n/a	Involved in the study
☒	☐ ChIP-seq
☒	☐ Flow cytometry
☒	☐ MRI-based neuroimaging